Article

Hydrogen-Rich Syngas Production via Dry and Steam Reforming of Methane in Simulated Producer Gas over ZSM-5-Supported Trimetallic Catalysts

John Tamunosaki Iminabo [1,2,*], **Misel Iminabo** [1,2], **Alex C. K. Yip** [1] and **Shusheng Pang** [1,*]

[1] Department of Chemical and Process Engineering, University of Canterbury, Christchurch 8041, New Zealand
[2] Department of Chemical/Petrochemical Engineering, Rivers State University,
    Port Harcourt PMB 5080, Nigeria
*   Correspondence: john.iminabo@pg.canterbury.ac.nz (J.T.I.); shusheng.pang@canterbury.ac.nz (S.P.)

Abstract: This study investigated the production of hydrogen-rich syngas from renewable sources using durable and efficient catalysts. Specifically, the research focused on steam methane reforming (SRM) and dry methane reforming (DRM) of simulated producer gas from biomass steam gasification in a fluidized bed reactor. The catalysts tested are ZSM-5-supported nickel-iron-cobalt-based trimetallic catalysts in different ratios, which were prepared via the wet impregnation method. Synthesized catalysts were characterized using XRD, BET, H_2-TPR, and SEM techniques. The results of the SRM with the simulated producer gas showed that the 20%Ni-20%Fe-10%Co/ZSM-5 trimetallic catalyst, at a gas hourly space velocity (GHSV) of 12 $L \cdot h^{-1} \cdot g^{-1}$ and reaction temperature of 800 °C, achieved the highest CH_4 conversion (74.8%) and highest H_2 yield (65.59%) with CO_2 conversion (36.05%). Comparing the performance of the SRM and DRM of the simulated producer gas with the 20%Ni-20%Fe-10%Co/ZSM5 at a GHSV of 36 $L \cdot h^{-1} \cdot g^{-1}$ and 800 °C, they achieved a CH_4 conversion of 67.18% and 64.43%, a CO_2 conversion of 43.01% and 52.1%, and a H_2 yield of 55.49% and 42.02%, respectively. This trimetallic catalyst demonstrated effective inhibition of carbon formation and sintering, with only 2.6 wt.% carbon deposition observed from the thermo-gravimetric analysis of the used catalyst from the SRM of the simulated producer gas, thus promoting the potential of the ZSM-5-supported trimetallic catalysts in methane reforming.

Keywords: trimetallic catalyst; dry methane reforming (DRM); steam methane reforming (SRM); titanomagnetite; ZSM-5 support

1. Introduction

The heavy reliance on fossil fuels in the world, fuel price uncertainties, and induced greenhouse gas (GHG) emissions are among many global challenges for mankind [1–4]. These challenges, combined with the constantly rising demand for energy, have stimulated research on alternative renewable sources of energy, of which biomass has been found to be one of the most attractive sources for producing fuels and chemicals, owing to its abundant availability and renewability [5,6].

Several pathways to generating energy from biomass have been developed, and these pathways can be classified into two categories: thermochemical (combustion, pyrolysis, gasification, and liquefaction) and biological conversion (digestion, fermentation). Through these pathways of biomass conversion, different energy products can be produced, which include electricity, liquid fuels (ethanol, bio-oil), solid fuels (charcoal or bio-char), and gaseous fuels like hydrogen and syngas [3,6]. To produce hydrogen and syngas from biomass, pyrolysis and gasification are preferred first step in conversion technologies, followed by reforming reactions [5,7].

In the gasification of biomass, using steam as the gasification agent can achieve high hydrogen yield and hydrogen content in the producer gas. The producer gas from biomass

steam gasification also contains CH_4, CO, and CO_2, among other gases [7,8]. The producer gas from the gasification of biomass using air as the gasification agent contains a high concentration of nitrogen; however, the nitrogen content is greatly reduced when steam is used as the gasification agent [8,9]. To increase hydrogen yield, the CH_4 and CO in the producer gas can be converted to hydrogen and CO_2 through reforming and water–gas shift reactions, while CO_2 can also be captured for reuse [3,5]. However, if the target application of the producer gas is for liquid fuel production through Fischer–Tropsch synthesis, a high H_2 content and a H_2/CO ratio of two are preferred. Therefore, technologies for the gas processing and the conversion of CH_4 are being actively developed [10]. Such technologies include the steam reforming of methane (SRM), the dry reforming of methane (DRM), or their combined form, known as combined steam and dry reforming of methane (CSDRM) [10]. Both SRM and DRM reactions are endothermic, and are described by Reactions (R1) and (R2), respectively, as follows.

$$CH_{4(g)} + H_2O_{(g)} \leftrightarrow CO_{(g)} + 3H_{2(g)} \qquad \Delta H^0 = 206 \text{ (kJ/mol)} \qquad \text{(R1)}$$

$$CH_{4(g)} + CO_{2(g)} \leftrightarrow 2CO_{(g)} + 2H_{2(g)} \qquad \Delta H^0 = 248 \text{ (kJ/mol)} \qquad \text{(R2)}$$

The SRM process is a well-known process that has been used for several decades in hydrogen production from natural gas, and is reported to account for over 50% of produced hydrogen. However, it is faced with issues of catalyst selection due to problems of sintering and coke formation, leading to catalyst deactivation [11,12]. The development of suitable and thermally stable catalysts with minimal coke deposition and improved CH_4 conversion is part of ongoing research in hydrogen production using the SRM technique. On the other hand, DRM, which involves the direct reaction of CH_4 and CO_2 to produce H_2 and CO, also encounters challenges with coke formation and sintering [11]. Consequently, finding the right catalyst for these reforming processes to mitigate the aforementioned challenges is of great importance, and is the objective of several researchers.

It is well known that noble metal catalysts like Pt, Pd, and Rh have high catalytic activity and carbon formation resistance; however, they have minimal applications industrially due to their high cost and limited resources [13–16]. The high cost of these materials prompted research on less expensive and readily available transition-metal-based catalysts like Ni, Co, and Fe [14,16,17]. These transition metals, especially Ni-based metals, have become the most used catalysts for SRM and DRM. However, Ni-based catalysts—though they are highly active and compare favorably with some noble metals—suffer deactivation due to carbon deposition and sintering. To minimize the challenges of Ni-based metals, researchers have developed different strategies, such as reducing Ni particle size, alloying, doping promoters, and using basic, dual, or structured supports, etc. [14–20].

It has been reported that when Ni forms an alloy with other metals, its resistance toward carbon deposition is remarkably improved, with an increase in reducibility and dispersibility of the Ni [21]. A typical example is the Ni-Fe bimetallic alloy catalysts, with high performance for SRM and DRM [19,22,23].

Theofanidis et al. synthesized a novel $MgFe_xAl_{2−x}O_4$ spinel as support for Ni catalysts and developed a Ni-Fe alloyed catalyst supported by carefully tuning $MgFe_xAl_{2−x}O_4$, which showed enhanced coke resistance during the CSDRM process [20].

Tsodikov et al. in their work applied an Al_2O_3-supported Ni-Fe catalyst to the steam reforming of methane [24]. The results from their work showed improved catalyst activity, performance stability, low coke formation, and resistance to deactivation by hydrogen sulphide that was present in the reaction gas mixture [24]. Djaidja et al. in their work prepared and applied Ni-Fe and Ni-Cu catalysts supported by MgO and Mg-Al for SRM and DRM [25]. The presence of a Ni-Fe alloy enhanced the catalyst reactivity with very high performances (with high CH_4 conversion, high H_2 yield, and high CO yield) and a good resistance to coke formation [25].

Estephane et al. applied Ni-Co/ZSM5 for DRM. They reported a 60% methane conversion and a low carbon deposition due to the presence of a Ni-Co alloy. They stated

that the oxidative property of Co influenced carbon gasification [26]. Siang et al. synthesized a bimetallic 5%Ni-10%Co/Al_2O_3 catalyst using the impregnation method and evaluated its performance for methane-reforming reactions at different reaction temperatures (650–700 °C). They reported a 67% methane conversion at 700 °C with the deposition of filamentous carbon [27]. You et al. in their work prepared Ni-Co/Al_2O_3 bimetallic catalysts for SRM. They stated in their results that the addition of Co, which formed the Ni-Co alloy, significantly improved the coke resistance and the reaction stability with a mild loss of the reforming activity [28]. Wu et al. employed an alumina-supported Ni-Co catalyst for the DRM. They reported high catalytic activity, as the presence of Co was reported to influence the usual RWGS that occurs as a side reaction during DRM [29].

Enhanced catalytic performances, due to the synergy between transition metals and with other metals, gave rise to the development of trimetallic catalysts for higher activity, minimization of carbon deposition, and increased yield [30]. Jin et al. [16] reported on the application of supported trimetallic alloy Ni-Fe-Cu_m-$Mg_xAl_yO_z$ as a DRM catalyst. The study showed that the trimetallic alloy material exhibited improved stability during the DRM process. Specifically, the presence of Fe in the trimetallic catalysts was found to be far more stable than in bimetallic catalysts [16]. Al-doghachi et al. used Ni-Pt-Pd/MgO trimetallic catalysts for DRM and reported increased catalyst activity, thermal stability and decreased carbon deposition [31]. Kozonoe et al. in their work applied the Fe-Co-Cu trimetallic catalyst supported on MWCNT for the reforming of methane and CO_2, and reported good thermal stability and high activity in the catalyst with very low carbon formation [32]. Zhang et al. developed and applied Cu-Ni-Pt ternary alloy clusters and reported high catalytic activity [33]. Zhang et al. in their work applied the Ni-Fe-MgO catalyst for DRM and reported on the efficient carbon-resistant property of Fe in the catalyst [34].

Supports play an integral role in catalysts, and should not be viewed independently, as they serve as the literal foundation for the catalytically active metal. Their function is crucial in achieving both stability and a high amount of active surface area. Commonly used supports for methane reforming are $\alpha-$ and $\gamma-Al_2O_3$, MgO, $MgAl_2O_4$, ZSM-5, SiO_2, TiO_2, ZrO_2, and La_2O_3. Due to their favorable porosity and surface area, these supports facilitate prolonged contact between the reactants and catalyst, leading to enhanced reaction efficiency [26,35].

Zeolites serve as highly efficient microporous catalysts suitable for supporting methane reforming. Their distinctive morphological characteristics encompass uniform pores, well-defined crystalline structures, impressive thermal stability, and substantial specific surface areas [35]. Gao et al. in their work developed and applied ZSM-5-supported Ni-Ce catalysts for CSDRM; they reported a high catalyst activity and very low carbon deposition, which they ascribed not just to the efficiency of the Ce promoter, but also to the large surface area and microporous structure of ZSM-5, as it aided metal-support interaction and inhibited carbon formation [36]. Results from the works of Estephane et al. [26], Ahmed et al. [37], and Majewska et al. [38] support the assertion of Gao et al. [36] on the efficiency of ZSM-5 as a support for steam-reforming processes.

Despite extensive research, the primary challenges with catalysts in the SRM and DRM processes remain carbon deposition and low syngas quality. To address these issues effectively and achieve a more suitable H_2/CO gas ratio with the aim to facilitate the production of extended hydrocarbon chains or to oxygenate chemicals through the Fischer–Tropsch process, researchers are exploring the combination of SRM and DRM [39]. This study aims to investigate this combination, which has the potential to mitigate environmental concerns and produce valuable syngas. The experimental investigation employs Ni-Fe-Co/ZSM-5 trimetallic catalysts to convert methane and carbon dioxide in producer gas from biomass gasification into syngas by incorporating steam.

The use of ZSM-5-supported Ni-Fe-Co trimetallic catalysts has not been reported in the literature for dry and/or steam reforming of methane. This study provides a fresh perspective on the two reaction systems (SRM and DRM) by exploring the synergistic

impact of Ni, Fe, and Co on ZSM-5 support in methane reforming. Various characterization methods were employed to gain insights into the catalysts' composition and structure, which in turn, enhanced our understanding of their activity.

2. Materials and Methods

2.1. Catalysts Preparation

In this study, Ni-Fe-Co trimetallic catalysts supported by ZSM-5 were synthesized using the wet impregnation method. All the chemicals utilized were of analytical grade. The calculated weights of the metal precursors $Fe(NO_3)_3 \cdot 9H_2O$, $Ni(NO_3)_2 \cdot 6H_2O$, and $Co(NO_3)_2 \cdot 6H_2O$ were dissolved in deionized water. Then, a calculated amount of the ZSM-5 was added depending on the pre-set catalyst formula. Once this was performed, the solution was subjected to constant stirring (using a magnetic stirrer) at 90 °C for 3 h to form a homogenous paste, which was finally dried at 110 °C for 12 h. The dried mixture was then calcined at 650 °C for 4 h in a muffle furnace. The formulas were, respectively, 10%Ni-20%Fe-20%Co (10Ni/ZSM-5), 20%Ni-20%Fe-10%Co (10Co/ZSM-5), and 20%Ni-10%Fe-20%Co (10Fe/ZSM-5). This is the elemental weight composition in the calcined catalysts.

The ZSM-5 used in this work has a Si/Al ratio of 25, and total acidic sites were determined to be 0.358 mmol/g using ammonia temperature programmed desorption.

2.2. Test Gases

Reactant feed gases used in the experiments were as follows: (i) Pure methane (99.85 vol.%) and steam; (ii) Simulated producer gas and steam. The simulated producer gas was comprised of 21.2 ± 0.4 vol.% CO, 20.5 ± 0.4 vol.% CO_2, 15.5 ± 0.3 vol.% CH_4, and the remaining was H_2. The composition of the clean (pollutant-free) simulated producer gas was selected based on the producer gas composition from biomass steam gasification in a 100 kW dual fluidized bed DFB gasifier developed in this research group at the University of Canterbury, New Zealand [40].

2.3. Experimental System and Method

Experiments were conducted in a fluidized bed reactor (ID 52 mm and L 800 mm) as illustrated in Figure 1. The fluidized bed reactor consists of a preheating zone and a reaction zone. Within the reactor, a 3 mm thick quartz-fritted disc is placed at the position of the two-zone connection to hold the catalysts. Heat for the reactor is provided by a set of electrical elements that are lined along the length of the reactor, protected by an external housing. The temperature in the different zones of the reactor is controlled by proportional controllers. A thermocouple is fitted on the top flange of the reactor, which allows for the bed temperature to be measured.

The particle size of the calcined catalysts used in this study is 215 μm. Prior to each experiment, the calculated amount of the catalyst (based on the required GHSV) was in situ reduced under a 5% H_2 flow (40 mL/min) at 600 °C for 120 min, followed by flushing with N_2 for 20 min. Then, the reactor was heated at a controlled heating rate to the target reaction temperatures, which were 700, 750, and 800 °C, respectively. When the reactor temperature reached the target reaction temperature and was stable, the reactant gas mixture was introduced into the reactor. The fluidizing gas (reactant gas mixture) flowrate was based on the minimum fluidization velocities determined earlier for each catalyst. The operation pressure was controlled to be slightly above the atmosphere.

De-ionized water was pumped into a heated mixing chamber which temperature was controlled at 200 °C and the steam generated was then mixed with either the pure methane or the simulated producer gas. A steam to methane mole ratio of 3 was used in all the SRM experiments, as ratios above the stoichiometric ratio have been reported to be beneficial for hydrogen yield and coke minimization [36], while in the DRM experiments, only simulated producer gas was injected without steam.
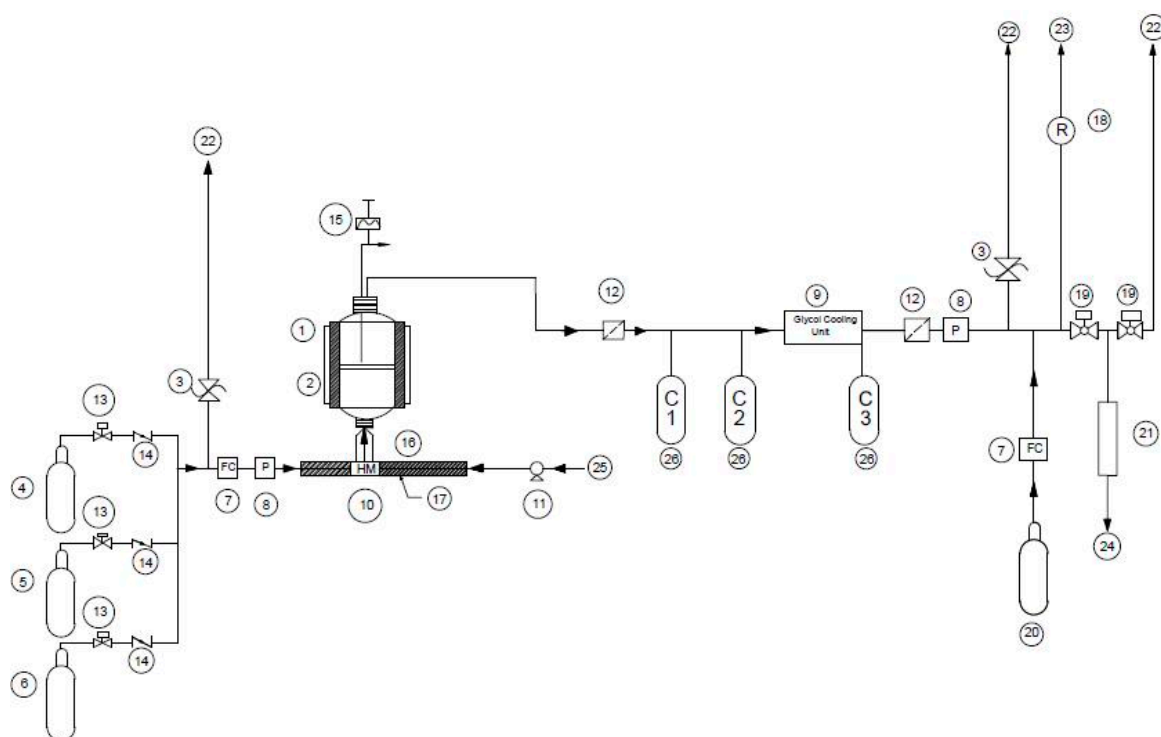
Figure 1. Experimental set-up. (1) Fluidized bed reactor; (2) Electric heaters; (3) Pressure relief valve; (4) N_2 gas bottle; (5) 5%H_2 in Nitrogen; (6) CH_4 and simulated producer gas stand; (7) Flowmeter; (8) Pressure gauge; (9) Glycol cooling unit; (10) Heated mixing chamber; (11) Pump; (12) Filter; (13) Gas valve; (14) Check valve; (15) Thermocouple; (16) Heating element; (17) Heater control unit; (18) Rotameter; (19) Ball valves; (20) Helium gas; (21) SPE column; (22) Vent; (23) Flue gas furnace; (24) Micro GC; (25) Water; (26) Condenser.

In the SRM experiments, excess steam was condensed and collected in the condensers after passing through a glycol cooling unit in the experimental system. Helium gas (inert) was added at 0.15 L/min to the product gas stream after the reactor, but in the upstream of the sample collection port to aid the determination of the product gas flowrate. The product gas containing helium was analyzed with the Agilent Micro GC, from which the gaseous species of He, H_2, CH_4, and CO were detected in the Molsieve 5Å column, while CO_2 was detected in the Poraplot column. For reliability, each experiment was performed in triplicates, and the average values were used in subsequent calculations for CH_4 and CO_2 conversions, as well as H_2 yield using the following equations:

1. Conversion,

$$X = \frac{(flowrate\ in - flowrate\ out)}{flowrate\ in} 100\% \tag{1}$$

2. Hydrogen yield,

$$Y_H = \frac{Actual\ yield}{Theoritical\ expected\ yield} 100\% \tag{2}$$

3. Hydrogen selectivity,

$$S_H = \frac{Hydrogen\ Yield}{Conversion,\ CH_4} 100\% \tag{3}$$

Theoretical expected hydrogen yield was calculated based on the stoichiometry in Reaction (R1) for SRM and Reaction (R2) for DRM. SRM experiments were first conducted using pure methane and steam, using the three ZSM-5-supported catalysts to determine the effect of metal precursor concentration on CH_4 conversion and H_2 yield. The catalyst with the highest CH_4 conversion and H_2 yield among the three ZSM-5-supported catalysts

during the pure methane steam reforming was chosen and used in subsequent catalytic tests. The effect of gas hourly space velocity (GHSV) on CH_4 conversion and H_2 yield was examined using the simulated producer gas. In all SMR experiments, the GHSV is based on the combined steam and methane or steam and simulated producer gas flowrates. The GHSVs used for the different catalytic tests are given in each section.

2.4. Catalyst Characterization

The catalysts' surface area, pore diameter, and total pore volume were determined in this study using the nitrogen adsorption-desorption method. The measurements were conducted at a liquid nitrogen temperature of $-196.15\,°C$ with a Quantachrome Instruments Autosorb iQ-XR model 7 surface analyzer. Prior to the N_2 adsorption measurements, the samples (50 mg) underwent degassing in a vacuum at 200 °C for 12 h. The surface area was calculated based on the Brunauer–Emmett–Teller (BET) method using the N_2 adsorption data. Additionally, the pore volume and average pore diameter were determined using the Barrett–Joyner–Halenda (BJH) adsorption method [41].

The hydrogen temperature programmed reduction (H_2-TPR) measurements were conducted using a BELCAT II Catalyst Analyzer 2.5 unit from MicrotracBEL Corporation equipped with a thermal conductivity detector (TCD). A 50 mg sample was subjected to degassing at 180 °C for 2 h in a pure helium atmosphere. Subsequently, the sample was transferred to the analysis port and subjected to a gradual heating process, ramping up to 1050 °C at a rate of 10 °C/min, with a reducing gas mixture (5% H_2/balance Ar) at a flow rate of 30 sccm. The amount of hydrogen uptake was measured based on the TCD response.

Powder X-ray diffraction (XRD) measurements of the reduced and used catalysts were performed in order to verify the chemical components present. The XRD patterns were determined using a Rigaku Smartlab X-ray diffractometer.

The scanning electron microscopy (SEM) technique was utilized to examine the surface morphology of both the fresh calcined and used catalysts. The SEM analysis was performed using a JEOL 7000F FE-SEM (JEOL Ltd., Tokyo, Japan) with a probe current of 7 mA and an acceleration voltage of 15 kV [41].

The coke deposition on the used catalyst surface was analyzed using thermal gravimetric analysis (TGA) in air, using a NETZSCH STA 499 thermal balance. The used catalyst was heated in the air from 40 °C to 1000 °C at a heating rate of 10 °C/min and an air flowrate of 50 mL/min.

3. Results and Discussion

3.1. Catalyst Characterization

3.1.1. X-ray Diffraction (XRD)

The phase identification for the three reduced ZSM-5-based Ni-Fe-Co trimetallic catalysts are presented in Figure 2. The diffraction peaks of Fe (JCPDS 06-0696), Co (JCPDS 15-0806), Ni (JCPDS 04-0850), Co-Ni (JCPDS 89-4307), CoFe (JCPDS 49-1567), and NiFe (JCPDS 47-1405) were observed. Also, the diffraction peaks of Fe-Ni-Co, Fe-Ni-Al, and FeO were noted. In addition, overlapping peaks were observed, as has been previously reported by Khan et al. [42]. The three catalysts (10Co/ZSM-5, 10Fe/ZSM-5, and 10Ni/ZSM-5) had similar species but varied in peaks. The presence of alloys and spinels indicate interaction between the transition metal components of the catalysts among themselves and with the support. Estephane et al. [26] and Wang et al. [43] have previously reported similar patterns.

3.1.2. Temperature Programmed Reduction (TPR)

The H_2-TPR profiles of the fresh calcined catalysts tested in this study are presented in Figure 3, showing three reduction peaks for the three Ni-Co-Fe/ZSM-5 catalysts. When the peaks were deconvoluted for the three catalysts, hydrogen consumption was determined to be between 0.218–0.531 mmol/g for peak one, 1.573–1.945 mmol/g for peak two, and

1–1.5 mmol/g for peak three. This shows that more reduction activity occurred at peaks two and three for the catalysts.
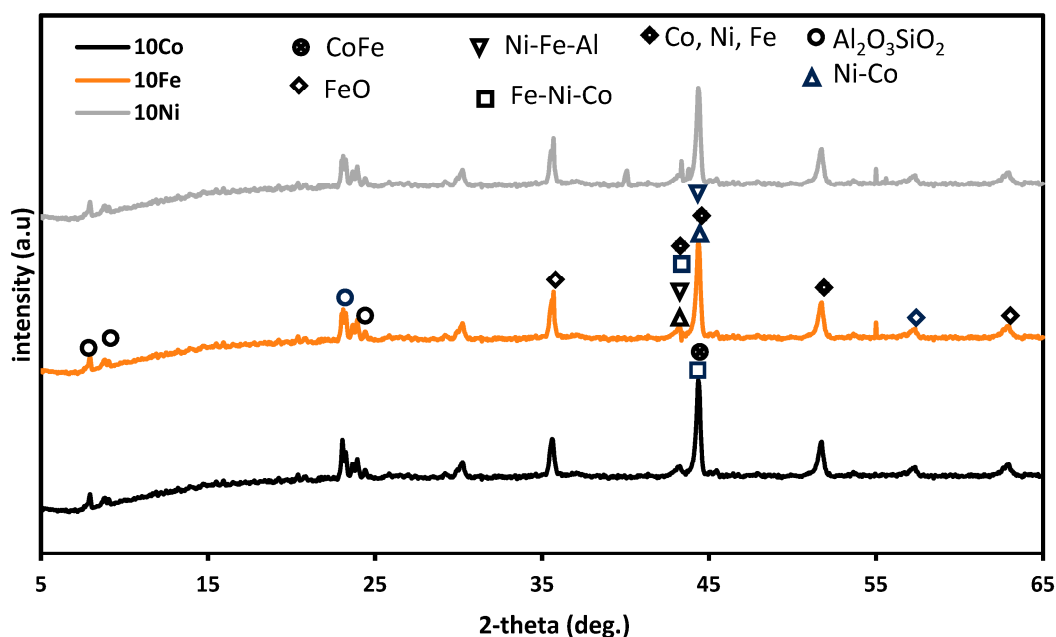

Figure 2. XRD profiles of the reduced three ZSM-5-supported Ni-Fe-Co catalysts.
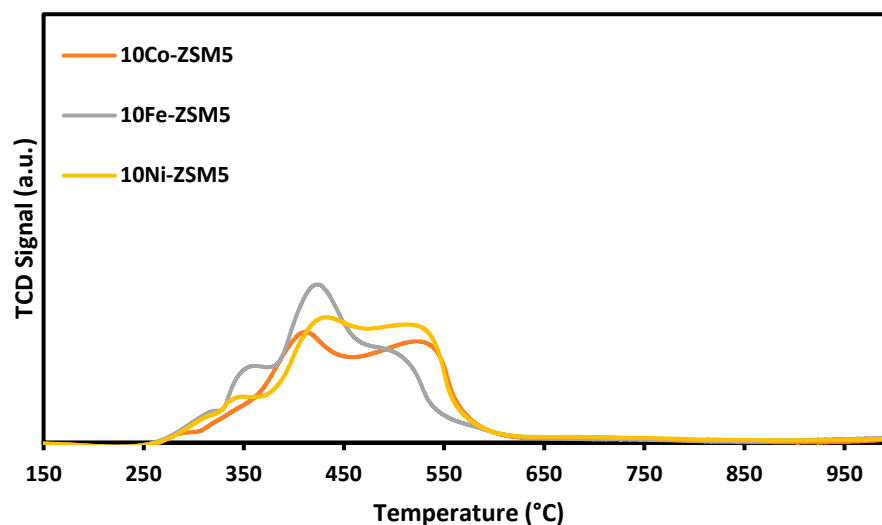

Figure 3. H$_2$-TPR profiles of the ZSM-5-supported trimetallic catalysts.

The low temperature reduction peaks up to 420 °C can be attributed to the reduction of metal oxides present in the catalyst, such as Fe$_2$O$_3$ to Fe$_3$O$_4$ and FeO, NiO to Ni°, and Co$_3$O$_4$ to Co, as these have weak interactions with the support. The higher temperature peak can be attributed to the reduction of the metal oxides formed based on stronger interactions among the transition metals. Such metal oxides are FeO, NiFe$_2$O$_4$, CoFe$_2$O$_4$, CoNiO$_3$, and Fe$_2$CoNiO$_4$. These metal oxides are reduced to form Fe, NiFe, CoFe, CoNi, and Fe-Ni-Co alloys. The results are consistent with the XRD analysis results discussed earlier in this paper, and consistent with those reported in the literature by Pudukudy et al. [44], Bayat et al. [45], and Estephane et al. [26].

3.1.3. N_2-Adsorption/Desorption Analysis

From the N_2 adsorption/desorption analysis, the surface and pore characteristics of the catalysts are presented in Table 1.

Table 1. Surface characteristics of the fresh calcined and reduced catalysts.

S/N	Catalyst	Surface Area (m²/g)	BJH Adsorption Pore Volume (cm³/g)	BJH Adsorption Pore Diameter (nm)
1	10Co-ZSM5	247	0.035	3
2	10Fe-ZSM5	211	0.037	3
3	10Ni-ZSM5	242	0.033	3
4	ZSM-5	417	0.051	2
5	Reduced 10Co-ZSM5	229	0.028	3

From Table 1, the average pore diameter of the calcined fresh trimetallic catalysts is 3 nm, which is within the mesoporous range (2–50 nm) [46]. Impregnation of the metals into the ZSM-5 increased the pore diameter, but reduced the surface area and pore volume due to the blocking of the pores by the metals. Estephane et al. [26] and GaO et al. [36] have reported similar results. The surface characteristics of the reduced 10Co-ZSM5 catalyst showed that reduction caused a decrease in surface area and pore volume.

3.2. Performance of Catalysts in Methane Reforming Reactions

3.2.1. SRM with Pure Methane as the Feeding Gas

Figure 4 shows the CH_4 conversion (Figure 4a), H_2 yield (Figure 4b), H_2 selectivity (Figure 4c), and H_2/CO ratio (Figure 4d) when the three ZSM-5-supported catalysts were used for the SRM reaction, with pure methane and steam as the feeding gas at three reaction temperatures of 700, 750, and 800 °C, a GHSV of 13.3 $L \cdot h^{-1} \cdot g^{-1}$, and a reaction time of 90 min. This test was carried out to determine the effect of metal precursor concentration and reaction temperature on CH_4 conversion and H_2 yield. From Figure 4a,b, it is found that the 10Co/ZSM-5 had the highest CH_4 conversion and the highest H_2 yield at the same reaction temperature. In Figure 4d, it is observed that the H_2/CO ratio decreased with an increase in temperature, although there was an increase in H_2 yield. This is due to the increase in carbon gasification, with an increase in temperature leading to the production of more CO, as the steam to methane mole ratio and GHSV was constant across the temperatures. The trend of results in Figure 4d agrees with the reported results of Maier et al. [47], Raju et al. [48], and Chibane et al. [49]. From Figure 4a,d, it can be seen that the results from the experiment follow similar trend as the calculated equilibrium data, although they vary in values. The result also shows that an increase in Ni and Fe concentrations and decrease in Co concentrations in the trimetallic catalysts favour CH_4 conversion and H_2 yield. This result has been previously reported by Jawad et al. [50] and Theofanidis et al. [51], who discovered that the Ni-Fe alloy, benefiting from the redox properties contributed by Fe, effectively suppresses carbon formation and enhances the metal–support interaction, resulting in improved dispersion, thus leading to higher catalyst activity. Ibrahim et al. [52] has also reported that an increase in Fe concentration increased the CH_4 decomposition and H_2 yield. Gao et al. [36] and Bayat et al. [53], based on their studies, reported a similar pattern of increased CH_4 conversion with an increase in Ni content in the catalysts up to 20% Ni, as in this study. They found that a low Ni concentration in the catalyst made it to be deficient in active sites on its surface and resulted in low activity. You et al. [28] reported in their work that the addition of Co to Ni improves metal dispersion and coke resistance, as it forms the Ni-Co alloy; however, they reported that increasing the Co content above 12% negatively affected the catalyst activity. Their findings affirm the result of this study. Takanabe et al. [54] in their work also found that increasing the Co content above 10% resulted in decreased CH_4 conversion. According to their findings, the formation of the Ni-Co alloy—though useful for reforming and coke

resistance—could obstruct a portion of the low-coordinated active Ni sites and diminish the metal dispersion, particularly when the Co content exceeds 10%. This phenomenon is considered to be the primary reason behind the reduced reforming activity observed in catalysts with a Co content of 20%.
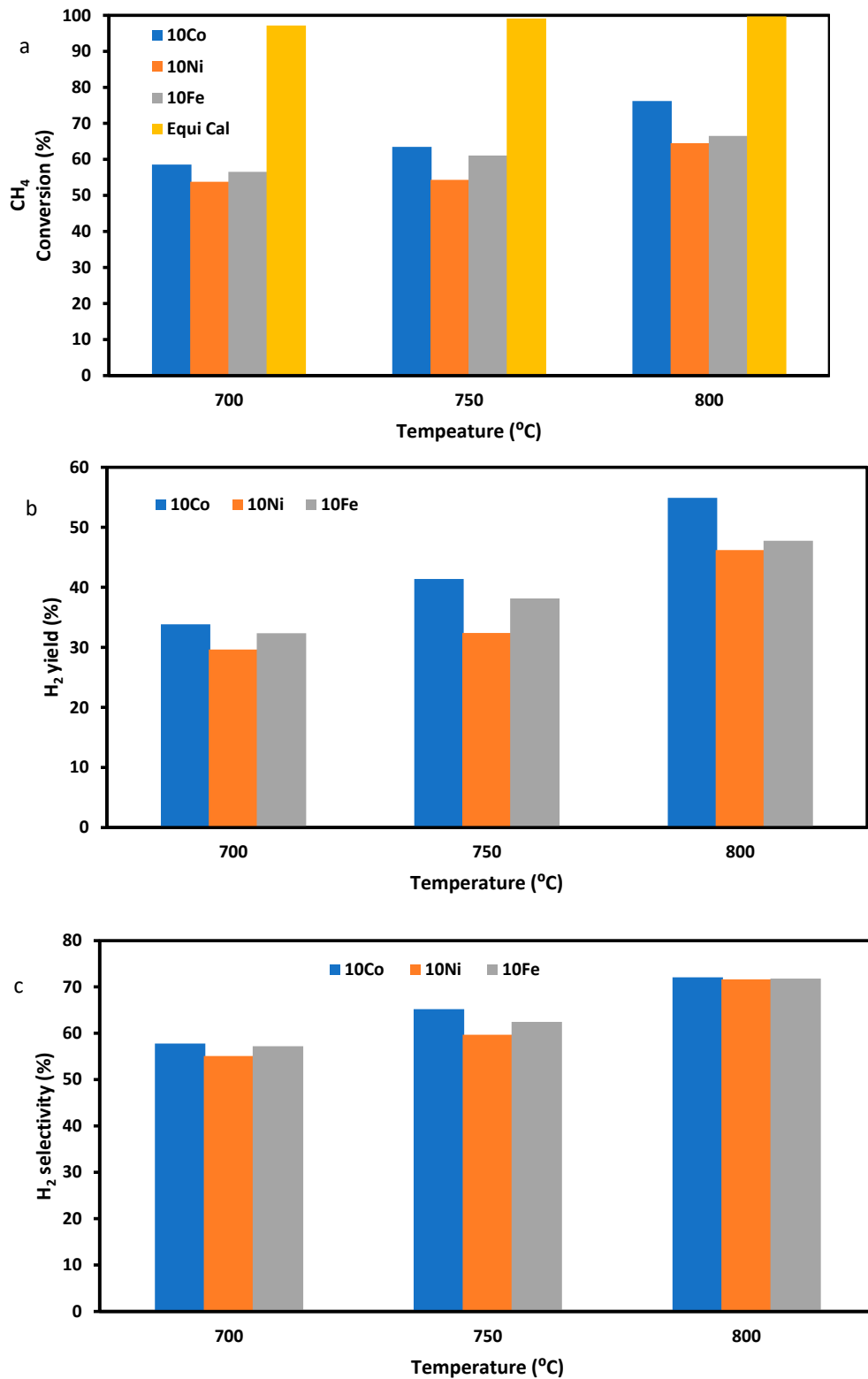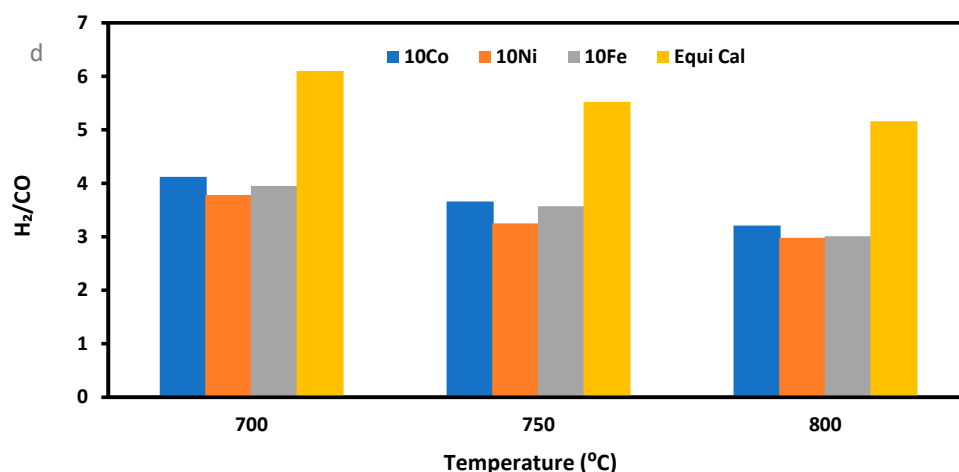

Figure 4. *Cont.*

Figure 4. Performances of the three ZSM-5 supported trimetallic catalysts in terms of (**a**) CH$_4$ conversion, (**b**) H$_2$ yield, (**c**) H$_2$ selectivity, and (**d**) H$_2$/CO ratio during the SRM of pure methane with H$_2$O/C = 3. Equi Cal is the calculated equilibrium data.

XRD analysis of the reduced and used 10Co/ZSM-5 in Figures 2 and 5 provides direct evidence on the formation of surface Ni-Fe and Ni–Co alloys, which play a critical role in minimizing coke formation by the catalyst, as the intensity of the carbon formed is low. The formation of Fe$_3$O$_4$ can be attributed to the oxidation of the FeO in the steam environment.
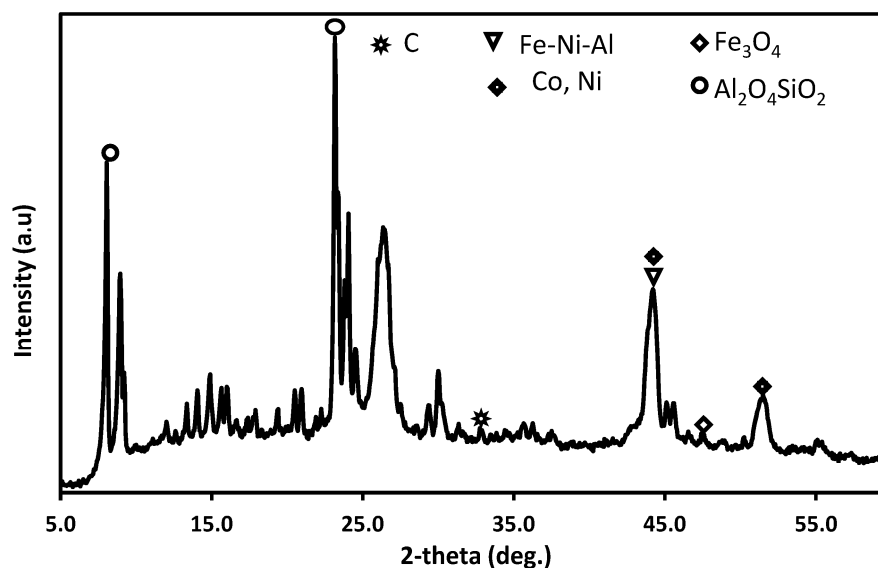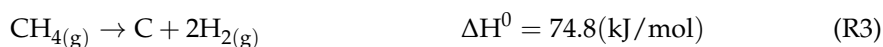

Figure 5. XRD profile of the used 10Co/ZSM-5 catalyst for the SRM of pure methane.

Based on the above results, the 10Co/ZSM-5 catalyst (20%Ni-20%Fe-10%Co/ZSM-5) was chosen for further tests.

From Figure 4, it is noted that an increase in temperature led to a corresponding increase in CH$_4$ conversion and H$_2$ yield. The increased CH$_4$ conversion and H$_2$ yield with reaction temperature is due to the increased decomposition of CH$_4$, which is an endothermic process and is favored by an increase in temperature (Reactions (R1) and (R3)). In Reaction (R3), carbon is deposited during the decomposition, and once this occurs, would lead to catalyst deactivation if sufficient steam is not available to react with the carbon. The reaction of carbon and steam, which is also endothermic and proceeds faster at higher temperatures, favours the generation of hydrogen and carbon oxides (Reaction (R4)).

The SRM Reaction (R1) is a reversible and endothermic reaction, which implies that a higher temperature would be thermodynamically and kinetically beneficial for the for-

ward reaction (reactant consumption) and increased rate of reaction [11,55]. The highest CH_4 conversion and H_2 yield in all the experiments was recorded at 800 °C. Thus, high temperatures favour the SRM.

$$CH_{4(g)} \rightarrow C + 2H_{2(g)} \qquad \qquad \Delta H^0 = 74.8 (kJ/mol) \qquad \text{(R3)}$$

$$H_2O_{(g)} + C \leftrightarrow H_{2(g)} + CO_{(g)} \qquad \Delta H^0 = 131.3 \ (kJ/mol) \qquad \text{(R4)}$$

3.2.2. Catalyst Stability Performance

The deactivation of catalysts employed in SRM and DRM is widely recognized to be influenced mainly by sintering and carbon formation. Sintering is a consequence of exposing the material to elevated temperatures, leading to the melting of certain components. On the other hand, carbon formation is associated with two distinct reactions: (1) CH_4 decomposition (Reaction (R3)), and (2) the Boudouard reaction (Reaction (R5)). To investigate the stability performance of the catalysts, the 10Co/ZSM-5 catalyst was tested for SRM using pure methane at a reaction temperature of 800 °C, a H_2O/CH_4 mol ratio of 3, and a GHSV of 13.3 $L \cdot h^{-1} \cdot g^{-1}$ for up to 180 min. The results are shown in Figure 6 for 60, 120, and 180 min of operation. During the reaction period of up to 180 min, the catalyst exhibited a consistent conversion ability, with CH_4 conversion remaining at 76.15–76.2% and a H_2 yield at 54.88–54.91%, respectively. These results confirm that no obvious deactivation occurred, thus the 10Co/ZSM-5 catalyst displayed robust resistance against sintering and carbon formation. However, further studies should be conducted beyond the time frame used in this study to determine the stability of the catalyst.
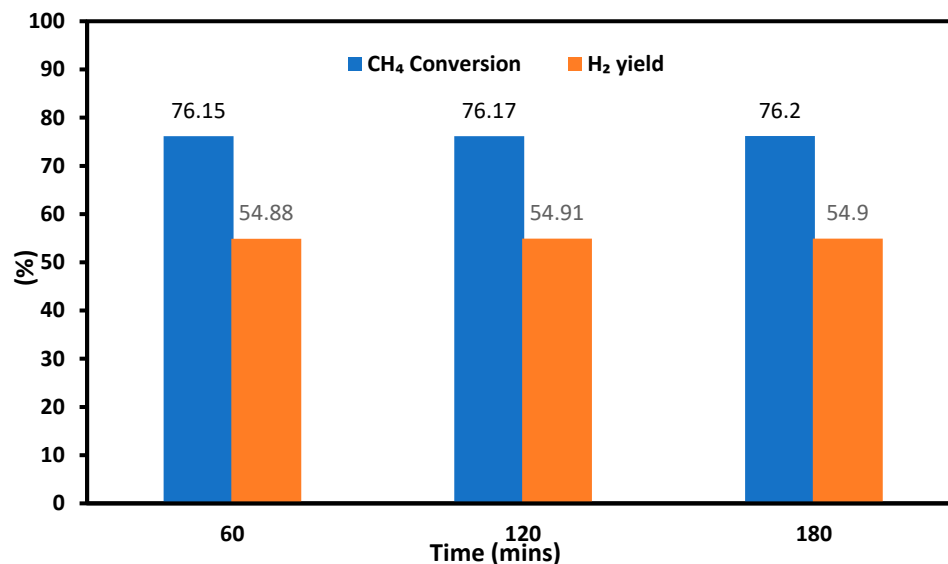
$$CO_{2(g)} + C \leftrightarrow 2CO_{(g)} \qquad \qquad \Delta H^0 = 172.4 \ (kJ/mol) \qquad \text{(R5)}$$

Figure 6. Stability performance of the 10Co/ZSM-5 for SRM with pure methane in respect to CH_4 conversion and H_2 yield with different reaction times.

3.3. Performance of Catalyst in the SRM of Simulated Producer Gas

Following the experiments on SRM with pure methane, simulated producer gas from biomass gasification was tested as the feeding gas, using the 10Co/ZSM-5 catalyst. This was carried out at a reaction temperature of 800 °C and a GHSV of 36 $L \cdot h^{-1} \cdot g^{-1}$. The results for CH_4 conversion, CO_2 conversion, and H_2 yield from this experiment are shown in Figure 7, which shows that the 10Co-ZSM5 catalyst achieved CH_4 conversion (67.18%), H_2 yield (55.49%), and CO_2 conversion (43.01%).
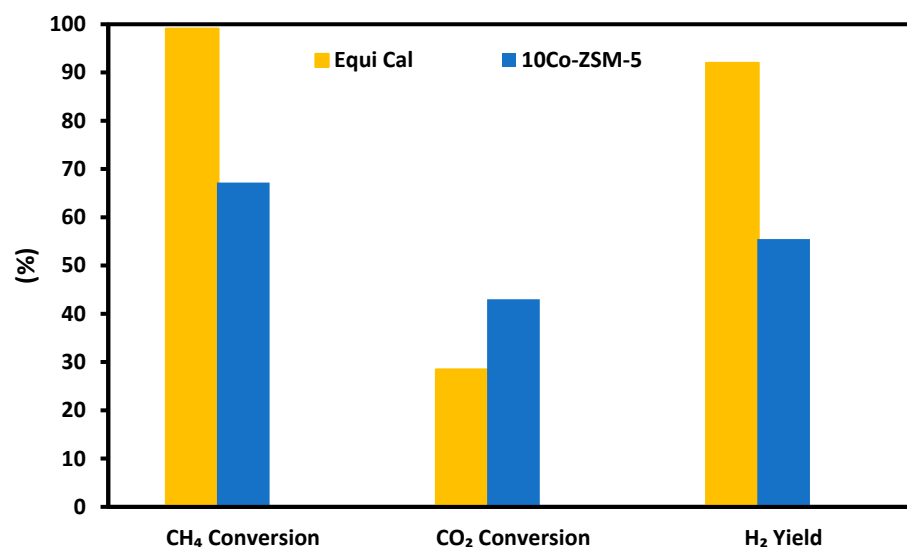
Figure 7. CH_4 conversion, CO_2 conversion, and H_2 yield in the SRM of a simulated producer gas with application of 10Co-ZSM5. Equi Cal refers to the calculated equilibrium data.

From the XRD of the used 10Co-ZSM5 catalyst for the SRM of simulated producer gas presented in Figure 8, carbon deposits and the formation of carbonates was noted. The carbonates were formed due to the reaction between the CO_2 present in the feed gas and the metals present in the catalysts in a steam environment. Also, the smaller intensity of the carbon that was formed indicates the prevalent occurrence of the reverse Boudouard reaction (Reaction (R5)) involving the CO_2 present in the feed gas and the oxidative ability of Co in the catalyst [26]. This process can be confirmed via the observed textural and morphological differences between the SEM images of the fresh catalysts and used catalysts in the SRM with pure methane, and the corresponding images with the simulated producer gas. This will be discussed in Section 3.6 of this paper.
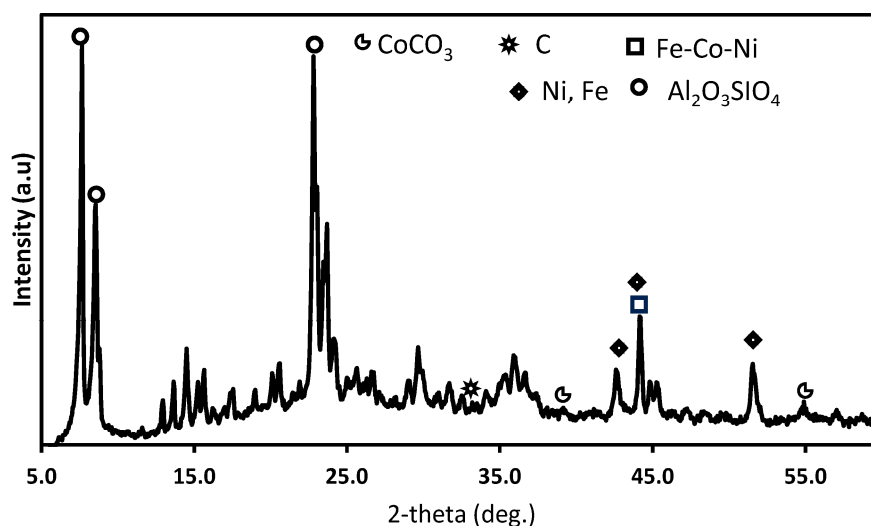

Figure 8. XRD profiles of the used 10Co/ZSM-5 catalyst used for the SRM of simulated producer gas.

3.4. Effect of Steam Feeding in the SRM

The processes using the simulated producer gas for SRM are a combination of SRM and DRM due to the presence of steam, CH_4, and CO_2 in the feed gas. The steam involvement in the SRM Reaction (R1) effectively increases the H_2 yield and H_2/CO ratio, which is desired for downstream gas application or the synthesis of liquid fuel through the Fischer–Tropsch process. However, a side reaction occurs at the SRM conditions, which is given in Reaction

(R2) as the dry methane reforming (DRM). This DRM is desirable if the processed gas is used for the Fischer–Tropsch process, but it may not be desirable if the target gas product is pure hydrogen. In order to understand the effect of the DRM reaction in the SRM process, experiments were carried out with the simulated producer gas at 800 °C and at a GHSV of 36 L·h^{-1}·g^{-1}, but without steam. The results of the DRM without steam and SRM with steam for the simulated producer gas using the 10Co-ZSM5 catalyst are presented in Figure 9. From the results, the conversion of CH$_4$ (67.18%) with the SRM was higher than with the DRM (64.43%). Also, the yield of hydrogen with the SRM (55.49%) was higher than that of the DRM (42.02%). This difference in conversion is due to the fact that for the SRM of the simulated producer gas, both Reaction (R1) and Reaction (R2) occurs. However, Reaction (R2) appears suppressed due to excess steam, while for the DRM, only Reaction (R2) is involved in the CH$_4$ conversion. Also, the higher CH$_4$ conversion can be attributed to the much higher CO$_2$ content in the feed gas when compared with the content of CH$_4$ in the feed gas. The results follow a similar trend as the calculated equilibrium data.
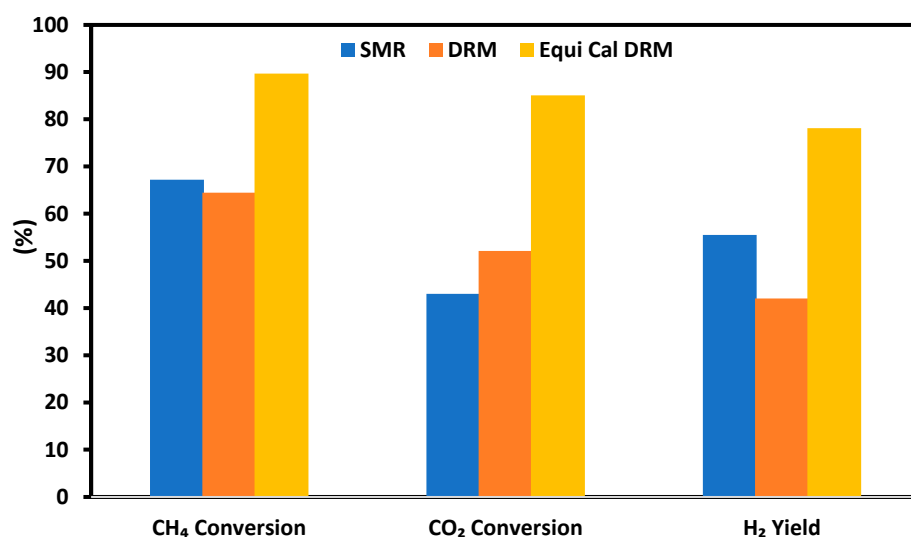

Figure 9. Effect of steam in methane reforming using simulated producer gas as the feeding gas. Equi Cal DRM refers to the calculated equilibrium data for the DRM process.

However, the conversion of CO$_2$ with the DRM (52.10%) was much higher than with the SRM (43.01%), as expected. In the SRM with steam available, the SRM reaction (R1) is more favourable than the DRM (R2) at the same temperature. However, for the DRM Reaction (R2) as a single reaction, CO$_2$ is involved as a direct reactant in the process, leading to its consumption. Also, a reverse water–gas shift reaction occurs as a side reaction, which consumes more CO$_2$ during the DRM [26]. These two reactions account for the increased CO$_2$ conversion during the DRM. These results show the desirability of the CSDRM, as it aids the utilization of two greenhouse gases (CH$_4$ and CO$_2$) and improves the yields of hydrogen and CO concurrently. Gao et al. [36], Batebi et al. [55], and Danilova et al. [56] have reported similar results.

3.5. Effect of Gas Hourly Space Velocity

For the SRM using the simulated producer gas, the effect of gas hourly space velocity (GHSV) was examined at 12, 24, and 36 L·h^{-1}·g^{-1}, respectively, for the 10Co/ZSM-5 catalyst at a reaction temperature of 800 °C. The results are shown in Figure 10, from which it is found that the CH$_4$ conversion and H$_2$ yield decreased while the CO$_2$ increased with increasing GHSV in the velocity range examined. This trend can be understood as the effect of residence time of the reactant gases being in contact with the catalyst.
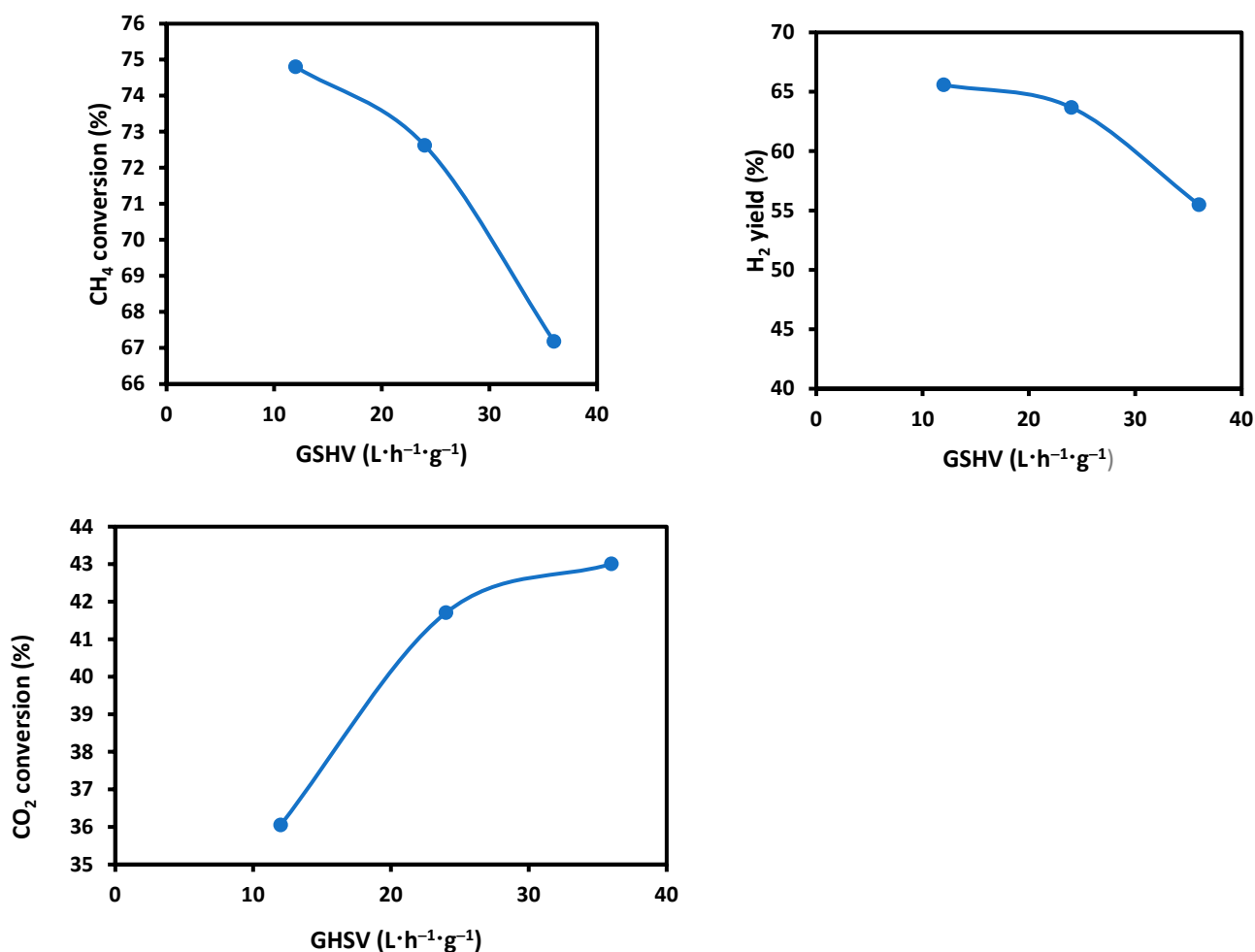
Figure 10. Effect of GHSV on CH_4 conversion, H_2 yield, and CO_2 conversion in the SRM using the simulated producer gas and 10Co/ZSM-5 catalyst at a reaction temperature of 800 °C.

A high GHSV means low residence time, which leads to a lower conversion of CH_4, while a lower GHSV favours a higher conversion of CH_4 to products, as the interaction period between the catalyst and CH_4 is longer. However, a contrast was observed with the CO_2 conversion where an increase in GHSV had a corresponding increase in CO_2 conversion. Gao et al. [36] and Schwengber et al. [57] have also reported a decrease in the conversion of CH_4 and an increase in CO_2 conversion with an increase in space velocity. They stated that although there was a decrease in CH_4 conversion, the CO_2 was involved in the conversion of deposited carbon with the reverse Bouodouard reaction. Also, the occurrence of the reverse water gas shift reaction will lead to a higher CO_2 conversion. Schwengber et al. [57] went on to say that the increase in CO_2 conversion with an increase in GHSV means that "CO_2 is not consumed in the final elementary steps of the reaction, since the adsorption and conversion of this reactant was further for higher space velocities". It was also noticed from the results that as GHSV increased, H_2 yield decreased. This is due to the decrease in CH_4 decomposition. Ullah et al. also reported on the inversely proportional relationship between GHSV and the H_2 yield [58].

3.6. Changes in Catalyst Characteristics through SRM and DRM

In previous sections, the XRD profiles of the used catalysts have been presented in Figures 5 and 8, and the results were discussed accordingly. The TGA technique was used to analyse and determine the carbon deposition on the used catalyst based on the weight change with heating. The used 10Co/ZSM-5 catalyst for the SRM with the simulated producer gas at 800 °C and 36 L·h^{-1}·g^{-1} was analyzed, and the result is shown in Figure 11.

From the figure, it is observed that a weight loss of 2.6% was recorded for the used 10Co/ZSM-5. This weight loss in the 10Co/ZSM-5 can be attributed to the loss of moisture and the combustion of the deposited carbon, and it is indicative of a relatively small amount of carbon. This outcome highlights the successful inhibition of carbon formation achieved by introducing Co and Fe to support Ni on ZSM-5, forming Ni-Fe and Ni-Co alloys. Furthermore, upon reaching 323 °C during the used 10Co/ZSM-5 analysis, a weight increase was observed due to the oxidation of active metals. Gao et al. [36] and Ibrahim et al. [52] have reported similar results.
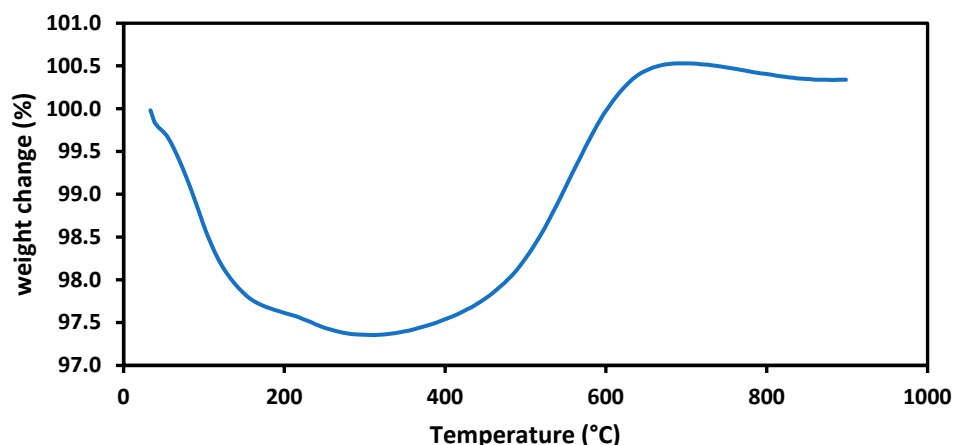

Figure 11. TGA curve for the used 10Co/ZSM-5 used for the SRM of simulated producer gas.

The textural properties and morphology of the fresh and used catalysts were examined using the scanning electronic microscopy (SEM) technique, and the results are presented in Figure 12. The SEM image of the fresh 10Co/ZSM-5 catalyst shows that the surface of the catalyst consists of more clustered crystallites and scattered pores.

The surfaces of the used 10Co/ZSM-5 catalysts with pure methane and simulated producer gas appear more coalesced than the fresh ones; however, the catalyst used with the pure methane appeared grainier than that with the producer gas.

The performance of the synthesised 10Co-ZSM5 catalyst used in this study (74.8% CH_4 conversion at a GHSV of 12 $L \cdot h^{-1} \cdot g^{-1}$ after 90 min at 800 °C) during SRM of simulated producer gas compare favourably with those reported in literature. For the Ni-Ce/ZSM-5 catalyst calcined at 800 °C, and used for CSDRM, Gao et al. [36] reported 89.6% CH_4 conversion and carbon deposition of 5 wt.% at 800 °C after 60 min reaction time at a GHSV of 7.2 $L \cdot h^{-1} \cdot g^{-1}$ while Estephane et al. [26] in applying the Ni-Co/ZSM5 catalyst for DRM reported a 60% CH_4 conversion and 5 wt% carbon deposition at 700 °C and 60 $L \cdot h^{-1} \cdot g^{-1}$. Also, the 30%Ni-Al$_2O_3$ catalyst produced and applied by Schwengber et al. [57] to the DRM process achieved a 50% CH_4 conversion at 30 $L \cdot h^{-1} \cdot g^{-1}$ and 700 °C reaction temperature whereas the 10Co-ZSM5 catalyst in this study achieved a 64.43% CH_4 conversion when it was used for the DRM process at 36 $L \cdot h^{-1} \cdot g^{-1}$. However, the difference in reaction conditions such as GHSV and catalyst particle size for the results reported in literature and the result of this work should be noted. The addition of promoters to the 10Co-ZSM5 would further enhance its performance to achieving the concentrations in the calculated equilibrium data [36].
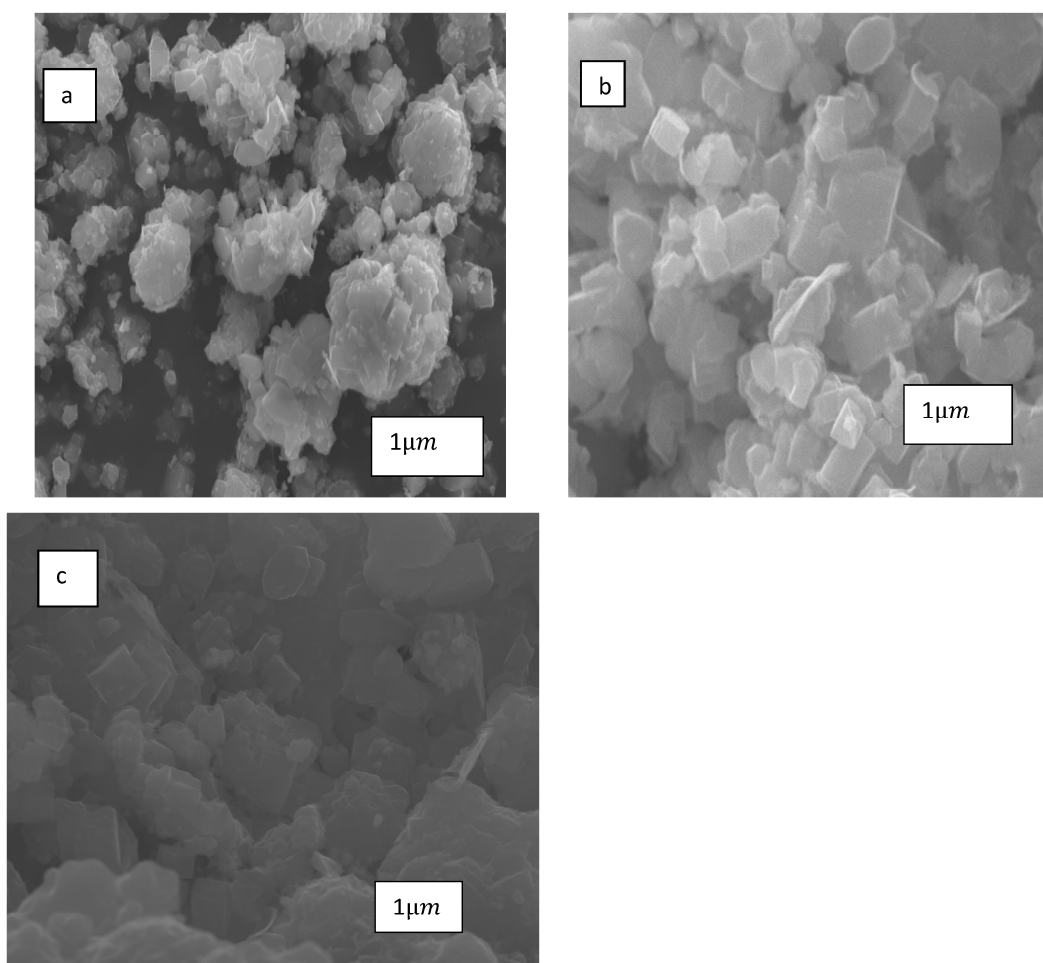
Figure 12. SEM images of: (**a**) fresh 10Co/ZSM-5, (**b**) used 10Co/ZSM-5 during SRM of pure methane, and (**c**) used 10Co/ZSM-5 during SRM of simulated producer gas.

4. Conclusions

Steam reforming of methane was carried out over trimetallic Ni-Fe-Co/ZSM-5 catalysts, with different Ni/Co/Fe ratios using pure methane gas and simulated producer gas, respectively. The results show that ZSM-5-supported Ni-Co-Fe catalysts are promising catalysts for processing biomass gasification producer gas for liquid fuel production through Fischer–Tropsch synthesis. The relatively large surface area and modified microporous structure of ZSM-5 improved the metal–support interaction and increased activity. The 10Co/ZSM-5 (20%Ni-20%Fe-10%Co-ZSM5) catalyst had the highest CH_4 conversion and H_2 yield among the tested trimetallic catalysts, confirming the effect of metal precursor concentration on catalyst activity. Additionally, results also show that the DRM occurring in the SRM of the producer may reduce carbon formation and enhance hydrogen yield.

TGA analyses of the used catalysts also revealed that the used 10Co/ZSM-5 catalyst had a relatively low carbon deposition (2.6 wt.%). This indicates that the alloying of Ni, Fe, and Co metals over ZSM-5 support inhibits carbon formation and sintering while promoting methane conversion and hydrogen yield.

Author Contributions: Conceptualization, J.T.I. and S.P.; Formal analysis, J.T.I., A.C.K.Y. and S.P.; Funding acquisition, S.P.; Investigation, J.T.I.; Methodology, J.T.I. and M.I.; Supervision, A.C.K.Y. and S.P.; Validation, J.T.I., M.I. and S.P.; Writing—original draft, J.T.I.; Writing—review and editing, M.I., A.C.K.Y. and S.P. All authors have read and agreed to the published version of the manuscript.

Data Availability Statement: Data are contained within the article.

Conflicts of Interest: The authors declare no conflict of interest.

References

1. Lee, H.; Kim, A.; Lee, B.; Lim, H. Comparative numerical analysis for an efficient hydrogen production via a steam methane reforming with a packed-bed reactor, a membrane reactor, and a sorption-enhanced membrane reactor. *Energy Convers. Manag.* **2020**, *213*, 112839. [CrossRef]
2. Mohamedali, M.; Henni, A.; Ibrahim, H. Hydrogen production from oxygenated hydrocarbons: Review of catalyst development, reaction mechanism and reactor modeling. In *Hydrogen Production Technologies*; Scrivener Publishing LLC: Beverly, MA, USA, 2017; pp. 1–76.
3. Peres, A.P.; Lunelli, B.H.; Maciel FIlho, R. Application of biomass to hydrogen and syngas production. *Chem. Eng. Trans.* **2013**, *32*, 589–594.
4. Chiari, L.; Zecca, A. Constraints of fossil fuels depletion on global warming projections. *Energy Policy* **2011**, *39*, 5026–5034. [CrossRef]
5. Lu, B.; Ju, Y.; Abe, T.; Kawamoto, K. Hydrogen-enriched producer gas production and chemical conversion to usable gas product through biomass gasification using NiO nanoparticles dispersed on SBA-15. *J. Nanosci. Nanotechnol.* **2017**, *17*, 6190–6197. [CrossRef]
6. Chang, A.C.; Chang, H.F.; Lin, F.J.; Lin, K.H.; Chen, C.H. Biomass gasification for hydrogen production. *Int. J. Hydrogen Energy* **2011**, *36*, 14252–14260. [CrossRef]
7. Parthasarathy, P.; Narayanan, K.S. Hydrogen production from steam gasification of biomass: Influence of process parameters on hydrogen yield—A review. *Renew. Energy* **2014**, *66*, 570–579. [CrossRef]
8. Hongrapipat, J. Removal of NH_3 and H_2S from Biomass Gasification Producer Gas. Ph.D. Thesis, University of Canterbury, Canterbury, New Zealand, 2014.
9. Speight, J.G. Types of gasifier for synthetic liquid fuel production: Design and technology. In *Gasification for Synthetic Fuel Production*; Woodhead Publishing: Cambridge, UK, 2015; pp. 29–55.
10. Chen, L.; Qi, Z.; Zhang, S.; Su, J.; Somorjai, G.A. Catalytic hydrogen production from methane: A review on recent progress and prospect. *Catalysts* **2020**, *10*, 858. [CrossRef]
11. Peiran, Z.; Abbas, T.; Dirk, P. Life cycle Assessment of hydrogen production via natural gas steam reforming vs. biomass gasification. *Preprints* **2022**, 2022010112. [CrossRef]
12. Torrez-Herrera, J.J.; Korili, S.A.; Gil, A. Recent progress in the application of Ni-based catalysts for the dry reforming of methane. *Catal. Rev.* **2021**, *65*, 1300–1357. [CrossRef]
13. De Llobet, S.; Pinilla, J.L.; Moliner, R.; Suelves, I. Relationship between carbon morphology and catalyst deactivation in the catalytic decomposition of biogas using Ni, Co and Fe based catalysts. *Fuel* **2015**, *139*, 71–78. [CrossRef]
14. Pakhare, D.; Spivey, J. A review of dry (CO_2) reforming of methane over noble metal catalysts. *Chem. Soc. Rev.* **2014**, *43*, 7813–7837. [CrossRef] [PubMed]
15. Rostrupnielsen, J.R.; Hansen, J.B. CO_2-reforming of methane over transition metals. *J. Catal.* **1993**, *144*, 38–49. [CrossRef]
16. Jin, F.; Fu, Y.; Kong, W.; Wang, J.; Cai, F.; Zhang, J.; Xu, J. Dry reforming of methane over trimetallic NiFeCu alloy catalysts. *Chem. Phys. Lett.* **2020**, *750*, 137491. [CrossRef]
17. Luisetto, I.; Tuti, S.; Di Bartolomeo, E. Co and Ni supported on CeO_2 as selective bimetallic catalyst for dry reforming of methane. *Int. J. Hydrogen Energy* **2012**, *37*, 15992–15999. [CrossRef]
18. Nair, M.M.; Kaliaguine, S.; Kleitz, F. Nanocast $LaNiO_3$ perovskites as precursors for the preparation of coke-resistant dry reforming catalysts. *ACS Catal.* **2014**, *4*, 3837–3846. [CrossRef]
19. Theofanidis, S.A.; Galvita, V.V.; Sabbe, M.; Poelman, H.; Detavernier, C.; Marin, G.B. Controlling the stability of a Fe–Ni reforming catalyst: Structural organization of the active components. *Appl. Catal. B Environ.* **2017**, *209*, 405–416. [CrossRef]
20. Theofanidis, S.A.; Galvita, V.V.; Poelman, H.; Dharanipragada, N.A.; Longo, A.; Meledina, M.; Marin, G.B. Fe-containing magnesium aluminate support for stability and carbon control during methane reforming. *ACS Catal.* **2018**, *8*, 5983–5995. [CrossRef]
21. Bian, Z.; Das, S.; Wai, M.H.; Hongmanorom, P.; Kawi, S. A review on bimetallic nickel-based catalysts for CO_2 reforming of methane. *ChemPhysChem* **2017**, *18*, 3117–3134. [CrossRef]
22. Kim, S.M.; Abdala, P.M.; Margossian, T.; Hosseini, D.; Foppa, L.; Armutlulu, A.; van Beek, W.; Comas-Vives, A.; Copéret, C.; Müller, C. Cooperativity and dynamics increase the performance of NiFe dry reforming catalysts. *J. Am. Chem. Soc.* **2017**, *139*, 1937–1949. [CrossRef]
23. Torimoto, M.; Sekine, Y. Effects of alloying for steam or dry reforming of methane: A review of recent studies. *Catal. Sci. Technol.* **2022**, *12*, 3375–3738. [CrossRef]
24. Tsodikov, M.V.; Kurdymov, S.S.; Konstantinov, G.I.; Murzin, V.Y.; Bukhtenko, O.V.; Maksimov, Y.V. Core-shell bifunctional catalyst for steam methane reforming resistant to H_2S: Activity and structure evolution. *Int. J. Hydrogen Energy* **2015**, *40*, 2963–2970. [CrossRef]

25. Djaidja, A.; Messaoudi, H.; Kaddeche, D.; Barama, A. Study of Ni–M/MgO and Ni–M–Mg/Al (M = Fe or Cu) catalysts in the CH_4–CO_2 and CH_4–H_2O reforming. *Int. J. Hydrogen Energy* **2015**, *40*, 4989–4995. [CrossRef]

26. Estephane, J.; Aouad, S.; Hany, S.; El Khoury, B.; Gennequin, C.; El Zakhem, H.; El Nakat, J.; Aboukaïs, A.; Abi Aad, E. CO_2 reforming of methane over Ni–Co/ZSM5 catalysts. Aging and carbon deposition study. *Int. J. Hydrogen Energy* **2015**, *40*, 9201–9208. [CrossRef]

27. Siang, T.J.; Singh, S.; Omoregbe, O.; Bach, L.G.; Phuc, N.H.H.; Vo, D.V.N. Hydrogen production from CH4 dry reforming over bimetallic Ni–Co/Al_2O_3 catalyst. *J. Energy Inst.* **2018**, *91*, 683–694. [CrossRef]

28. You, X.; Wang, X.; Ma, Y.; Liu, J.; Liu, W.; Xu, X.; Yuan, P.; Chen, X. Ni–Co/Al_2O_3 bimetallic catalysts for CH_4 steam reforming: Elucidating the role of Co for improving coke resistance. *ChemCatChem* **2014**, *6*, 3377–3386. [CrossRef]

29. Wu, Z.; Yang, B.; Miao, S.; Liu, W.; Xie, J.; Lee, S.; Pellin, J.; Xiao, D.; Su, D.; Ma, D. Lattice strained Ni-Co alloy as a high-performance catalyst for catalytic dry reforming of methane. *ACS Catal.* **2019**, *9*, 2693–2700. [CrossRef]

30. Crawley, J.W.; Gow, I.E.; Lawes, N.; Kowalec, I.; Kabalan, L.; Catlow, C.R.A.; Logsdail, J.; Taylor, S.H.; Hutchings, G.J. Heterogeneous trimetallic nanoparticles as catalysts. *Chem. Rev.* **2022**, *122*, 6795–6849. [CrossRef]

31. Al-Doghachi, F.A.; Rashid, U.; Taufiq-Yap, Y.H. Investigation of Ce (III) promoter effects on the tri-metallic Pt, Pd, Ni/MgO catalyst in dry-reforming of methane. *RSC Adv.* **2016**, *6*, 10372–10384. [CrossRef]

32. Kozonoe, C.E.; Bonfim, R.D.P.F.; Alves, R.M.B.; Schmal, M. The Fe-Co-Cu supported on MWCNT as catalyst for the tri-reforming of methane–investigating the structure changes of the catalysts. *Fuel* **2019**, *256*, 115917. [CrossRef]

33. Zhang, L.; Meng, Y.; Xie, B.; Xia, S. Theoretical investigation onto the reaction mechanism of dry reforming of methane on core–shell Cu-Ni-Pt ternary alloy clusters. *Chem. Phys. Lett.* **2021**, *781*, 138975. [CrossRef]

34. Zhang, T.; Liu, Z.; Zhu, Y.A.; Liu, Z.; Sui, Z.; Zhu, K.; Zhou, X. Dry reforming of methane on Ni-Fe-MgO catalysts: Influence of Fe on carbon-resistant property and kinetics. *Appl. Catal. B Environ.* **2020**, *264*, 118497. [CrossRef]

35. Dalena, F.; Giglio, E.; Marino, A.; Aloise, A.; Giorgianni, G.; Migliori, M.; Giordano, G. Steam reforming of bioethanol using metallic catalysts on zeolitic supports: An overview. *Catalysts* **2022**, *12*, 617. [CrossRef]

36. Gao, N.; Cheng, M.; Quan, C.; Zheng, Y. Syngas production via combined dry and steam reforming of methane over Ni-Ce/ZSM-5 catalyst. *Fuel* **2020**, *273*, 117702. [CrossRef]

37. Ahmed, T.; Xiu, S.; Wang, L.; Shahbazi, A. Investigation of Ni/Fe/Mg zeolite-supported catalysts in steam reforming of tar using simulated-toluene as model compound. *Fuel* **2018**, *211*, 566–571. [CrossRef]

38. Majewska, J.; Michalkiewicz, B. Production of hydrogen and carbon nanomaterials from methane using Co/ZSM-5 catalyst. *Int. J. Hydrogen Energy* **2016**, *41*, 8668–8678. [CrossRef]

39. Pour, A.N.; Mousavi, M. Combined reforming of methane by carbon dioxide and water: Particle size effect of Ni–Mg nanoparticles. *Int. J. Hydrogen Energy* **2015**, *40*, 12985–12992. [CrossRef]

40. Wang, Y. Removal of H_2S, NH_3 and Tars from the Producer Gas of Biomass Gasification by Secondary Measures. Ph.D. Thesis, University of Canterbury, Canterbury, New Zealand, 2018.

41. Iminabo, M.; Yip, A.C.K.; Iminabo, J.T.; Pang, S. High-temperature catalytic pyrolysis of radiata pine for production of high-value products. *Biomass Convers. Biorefinery* **2022**, 1–19. [CrossRef]

42. Khan, W.U.; Fakeeha, A.H.; Al-Fatesh, A.S.; Ibrahim, A.A.; Abasaeed, A.E. La_2O_3 supported bimetallic catalysts for the production of hydrogen and carbon nanomaterials from methane. *Int. J. Hydrogen Energy* **2016**, *41*, 976–983. [CrossRef]

43. Wang, I.W.; Kutteri, D.A.; Gao, B.; Tian, H.; Hu, J. Methane pyrolysis for carbon nanotubes and COx-free H_2 over transition-metal catalysts. *Energy Fuels* **2018**, *33*, 197–205. [CrossRef]

44. Pudukudy, M.; Yaakob, Z.; Akmal, Z.S. Direct decomposition of methane over SBA-15 supported Ni, Co and Fe based bimetallic catalysts. *Appl. Surf. Sci.* **2015**, *330*, 418–430. [CrossRef]

45. Bayat, N.; Rezaei, M.; Meshkani, F. Methane decomposition over Ni–Fe/Al_2O_3 catalysts for production of COx-free hydrogen and carbon nanofiber. *Int. J. Hydrogen Energy* **2016**, *41*, 1574–1584. [CrossRef]

46. Schwanke, A.J.; Balzer, R.; Pergher, S. Microporous and Mesoporous Materials from Natural and Inexpensive Sources. In *Handbook of Ecomaterials*; Torres Martínez, L.M., Kharisova, O.V., Kharisov, B.I., Eds.; Springer: Cham, Switzerland, 2017; Volume 136, pp. 3379–3399.

47. Maier, L.; Schädel, B.; Herrera Delgado, K.; Tischer, S.; Deutschmann, O. Steam reforming of methane over nickel: Development of a multi-step surface reaction mechanism. *Top. Catal.* **2011**, *54*, 845–858. [CrossRef]

48. Raju, A.S.; Park, C.S.; Norbeck, J.M. Synthesis gas production using steam hydrogasification and steam reforming. *Fuel Process. Technol.* **2009**, *90*, 330–336. [CrossRef]

49. Chibane, L.; Djellouli, B. Methane steam reforming reaction behaviour in a packed bed membrane reactor. *Int. J. Chem. Eng. Appl.* **2011**, *2*, 147. [CrossRef]

50. Jawad, A.; Rezaei, F.; Rownaghi, A.A. Highly efficient Pt/Mo-Fe/Ni-based Al_2O_3-CeO_2 catalysts for dry reforming of methane. *Catal. Today* **2020**, *350*, 80–90. [CrossRef]

51. Theofanidis, S.A.; Galvita, V.V.; Poelman, H.; Marin, G.B. Enhanced carbon-resistant dry reforming Fe-Ni catalyst: Role of Fe. *ACS Catal.* **2015**, *5*, 3028–3039. [CrossRef]

52. Ibrahim, A.A.; Fakeeha, A.H.; Al-Fatesh, A.S.; Abasaeed, A.E.; Khan, W.U. Methane decomposition over iron catalyst for hydrogen production. *Int. J. Hydrogen Energy* **2015**, *40*, 7593–7600. [CrossRef]

53. Bayat, N.; Rezaei, M.; Meshkani, F. COx-free hydrogen and carbon nanofibers production by methane decomposition over nickel-alumina catalysts. *Korean J. Chem. Eng.* **2016**, *33*, 490–499. [CrossRef]

54. Takanabe, K.; Nagaoka, K.; Nariai, K.; Aika, K.I. Titania-supported cobalt and nickel bimetallic catalysts for carbon dioxide reforming of methane. *J. Catal.* **2005**, *232*, 268–275. [CrossRef]

55. Batebi, D.; Abedini, R.; Mosayebi, A. Combined steam and CO_2 reforming of methane (CSDRM) over Ni–Pd/Al_2O_3 catalyst for syngas formation. *Int. J. Hydrogen Energy* **2020**, *45*, 14293–14310. [CrossRef]

56. Danilova, M.M.; Fedorova, Z.A.; Zaikovskii, V.I.; Porsin, A.V.; Kirillov, V.A.; Krieger, T.A. Porous nickel-based catalysts for combined steam and carbon dioxide reforming of methane. *Appl. Catal. B Environ.* **2014**, *147*, 858–863. [CrossRef]

57. Schwengber, C.A.; da Silva, F.A.; Schaffner, R.A.; Fernandes-Machado NR, C.; Ferracin, R.J.; Bach, V.R.; Alves, H.J. Methane dry reforming using Ni/Al_2O_3 catalysts: Evaluation of the effects of temperature, space velocity and reaction time. *J. Environ. Chem. Eng.* **2016**, *4*, 3688–3695. [CrossRef]

58. Ullah, K.S.; Omer, A.; Rashid, K.; Rehman, N.U.; Rahimipetroudi, I.; Kim, S.D.; Dong, S.K. Modeling and comprehensive analysis of hydrogen production in a newly designed steam methane reformer with membrane system. *Comput. Chem. Eng.* **2023**, *175*, 108278. [CrossRef]